Anisotropic diffusions in supercooled liquids

Jiankai Hu[1] and Ke Chen[1,2,3,*]

[1]*Beijing National Laboratory for Condensed Matter Physics and Laboratory of Soft Matter Physics, Institute of Physics, Chinese Academy of Sciences, Beijing 100190, China*

[2]*University of Chinese Academy of Sciences, Beijing 100049, China*

[3]*Songshan Lake Materials Laboratory, Dongguan, Guangdong 523808, China*

(Received 18 October 2024; revised 28 November 2025; accepted 11 December 2025; published 6 January 2026)

Using isoconfigurational ensemble simulations, we investigate the diffusion direction of individual particles in liquids in two dimensions. We find that the particle diffusion direction on the cage-jumping timescale is not random in the supercooled regime, and the diffusion anisotropy increases with decreasing temperature. Analyses of the simulations and colloidal experiments show that the diffusion anisotropy originates from the rise of the anisotropic local potential energy landscape. Particles prefer to move in directions with soft local stiffness during structural rearrangements. The structural evolution in supercooled liquids can thus be probabilistically predicted from the potential energy landscape that is determined by local structures.

DOI: 10.1103/575j-1k34

I. INTRODUCTION

Diffusion in normal liquids can be well modeled as random walks, with constant diffusion rates and random diffusion directions. In supercooled liquids or glasses, however, the diffusion rates become spatially heterogeneous, despite practically indistinguishable structures from those of equilibrium liquids. Many efforts have been made to understand this peculiar dynamical phenomenon in glassy systems [1–7]. Using isoconfigurational ensemble simulations, Widmer-Cooper, *et al.* confirm that the dynamical heterogeneity is inherently related to the structures of glasses [8]. Structural order parameters, including two-body structural entropy S_2 [9–11], medium-range crystalline order ψ_6 [9,12,13], and local packing order Θ [14], have been shown to correlate with particle mobilities in different systems. Most studies on the dynamics of glassy systems focus primarily on the rate of diffusion of the constituent particles, while the direction of diffusion is usually assumed to be completely random and unpredictable. On the other hand, some evidence suggests that particles in systems of slow dynamics may prefer to move in certain directions depending on local structures. For example, Chen, *et al.* find that particles in colloidal glasses tend to follow the direction of low energy soft modes during rearrangements [15,16]. In jammed granular packings, particles move toward the center of the local Voronoi polyhedron under external forces [17]. More recently, Xia, *et al.* discover that the orientational structural orders actually have greater impact on local dynamics than translational orders [18]. It is therefore reasonable to expect that the anisotropy in local structures may influence the direction of particle diffusions in supercooled liquids.

Structure-based prediction of relaxation details for individual particles in glassy materials, even only probabilistically, is significant, as it enables one not only to map out the evolution of a system with some degree of confidence, but to obtain a more realistic estimation for the distribution of configurations. However, identification of the diffusion anisotropy in supercooled liquids or glasses in experiments is challenging, because under thermal fluctuations the direction of motion in a single observation is not always the most likely direction under the same condition, and it is practically impossible to repeat an experiment with precisely the same initial configurations. Isoconfigurational ensemble simulations [8,14] provide an ideal solution for this difficulty by randomizing the initial momenta of individual particles in systems of identical initial structures, and reveal different evolutionary paths of the system.

In this paper, we investigate the directions of diffusion for particles in two-dimensional supercooled liquids by isoconfigurational ensemble simulations and colloidal experiments. We find that anisotropy in particle diffusions begins to develop in the supercooled regime, and increases with decreasing temperature. This anisotropy is most pronounced on the cage-jumping timescale, when the local structures are qualitatively changed. During cage jumping, particles are more likely to move in the directions with softer energy barriers. This is similar to the observation that fast dynamics are spatially correlated to low energy soft modes. However, diffusion anisotropy is not spatially correlated with the rate of dynamics. Our study reveals that the glassy dynamics contains more information than simply being fast or slow, and it is possible to probabilistically predict the evolution of glass structures.

II. SIMULATIONS AND EXPERIMENTS

We perform molecular dynamics simulations of a binary liquid in two dimensions [19,20]. The system consists of a mixture of particles of two species, A and B. The number ratio between A and B is 0.65:0.35. The mass of all the particles is m. The interaction potential is $V_{\alpha\beta} = 4\epsilon_{\alpha\beta}[(\sigma_{\alpha\beta}/r)^{12} -$

*Contact author: kechen@iphy.ac.cn

$(\sigma_{\alpha\beta}/r)^6]$ where $\epsilon_{AB} = 1.5\epsilon_{AA}$, $\epsilon_{BB} = 0.5\epsilon_{AA}$, $\sigma_{AB} = 0.8\sigma_{AA}$, and $\sigma_{BB} = 0.88\sigma_{AA}$. The simulations are performed in a square box of side length $L = 29.34$ with a total of 1000 particles under periodic boundary conditions. The system is first slowly cooled down (at the rate of -10^{-5}) from an equilibrium state at a sufficiently high temperature ($T_0 = 1.5$) to the target temperature $T_e = \{0.20, 0.30, 0.35, 0.40, 0.50, 0.60\}$. The system is then allowed to equilibrate at T_e before being quenched to the nearest inherent structure using the FIRE algorithm [21]. The configuration thus obtained is used as the initial configuration for the isoconfigurational ensemble simulations at T_e. For each initial configuration, 5000 isoconfigurational ensemble simulations are performed with random initial momenta drawn from a Maxwell-Boltzmann distribution for each particle.

In addition to simulations, we also perform colloidal experiments using temperature-sensitive poly(*N*-isopropylacrylamide) (PNIPAM) particles. The samples consist of a binary mixture of PNIPAM colloids confined between two coverslips, forming a monolayer. The size ratio of these two types of particles is ≈1.4 and the number ratio is ≈1. The packing fractions of the samples can be increased *in situ* by decreasing the temperature due to the thermal sensitivity of PNIPAM colloids [22]. The samples are continuously imaged using standard bright field microscopy for 1000 s at 60 fps. The trajectories of all particles are extracted using particle tracking software with a spatial resolution of ≈20 nm [23].

III. RESULTS

From the isoconfigurational ensemble simulations, we obtain 5000 trajectories for each particle under the same initial configuration. We examine the anisotropy in the positional distributions of individual particles at different cross sections of time. For perfectly isotropic diffusions, the positional distribution of an individual particle uniformly spreads out along all directions. For anisotropic diffusions, on the other hand, mirror symmetry is broken for certain directions. Specifically, we employ the skewness of the distribution, $s_i(\theta, t)$, to quantify the asymmetry in the positional distribution of a particle along a certain direction θ at time t, with θ being the angle relative to the x axis. The definition of $s_i(\theta, t)$ is

$$s_i(\theta, t) = \frac{\langle (x_{i,t,\theta} - \langle x_{i,t,\theta}\rangle)^3\rangle}{\langle (x_{i,t,\theta} - \langle x_{i,t,\theta}\rangle)^2\rangle^{3/2}}. \quad (1)$$

Here, $x_{i,t,\theta}$ is the projection of particle i's position at time t on direction θ, and $\langle ...\rangle$ represents the average over all the isoconfigurational runs. $s_i(\theta, t)$ is a dynamic quantity that takes into account many possible trajectories under the same condition. For isotropic distributions, $s_i(\theta, t)$ is zero for all θ. For a given t, the θ with the largest $s_i(\theta, t)$ or $s_{m,i}(t)$ indicates the direction along which the distribution of particle positions is most uneven. The colored contour plot in Fig. 1(a) shows an example of the distribution of positions extracted from the 5000 trajectories of the same particle at time t. The purple arrow indicates the direction along which the projected distribution is most skewed, as measured by $s_i(\theta, t)$. The distribution of the projected positions along the most skewed direction is plotted in Fig. 1(b), with clear asymmetry with respect to the

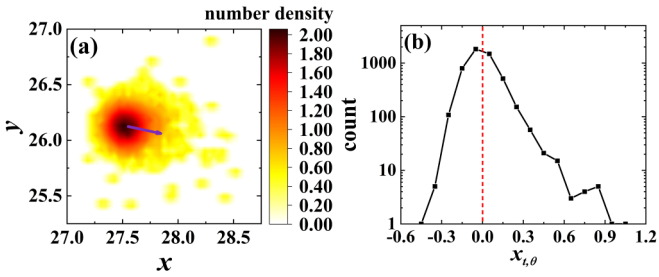

FIG. 1. (a) Positional distribution of a particle from isoconfigurational simulations (colored contour). The purple arrow indicates the direction where the distribution is most skewed. (b) The frequency distribution of the projections of the end points along the most skewed direction.

averaged position. When averaged over all the particles, the skewness $S_m(t) = \langle s_{m,i}(t)\rangle_i$ represents the overall degree of diffusion anisotropy in the system at time t.

Figure 2 plots the $S_m(t)$ as a function of time for different temperatures (solid lines). The anisotropy is low at short times, as the initial momenta for each particle are random in isoconfigurational simulations. The diffusion anisotropy increases with time and peaks around the cage-jumping timescale, indicated by the peak in the non-Gaussian parameter. The non-Gaussian parameter is defined as $\alpha_2(t) = \frac{\langle \Delta x^4\rangle}{3(\langle \Delta x^2\rangle^2)} - 1$ with Δx being the particle displacement during time interval t [3,24–26]. The peaks in the skewness indicate that the particle hopping directions are no longer random. Only after many successive hoppings, the random walk features of particle diffusions are recovered, when $S_m(t)$ begins to decrease at longer timescales. The diffusion anisotropy increases with decreasing temperature, as the anisotropy in the local potential energy landscape becomes significant compared to thermal fluctuations.

We examine the shape of the local potential energy landscape associated with the cage-jumping events in our simulations. We first determined the cage-jumping events by applying a hopping function to the trajectory of each particle [27,28]. The hopping function for particle i at time t is defined

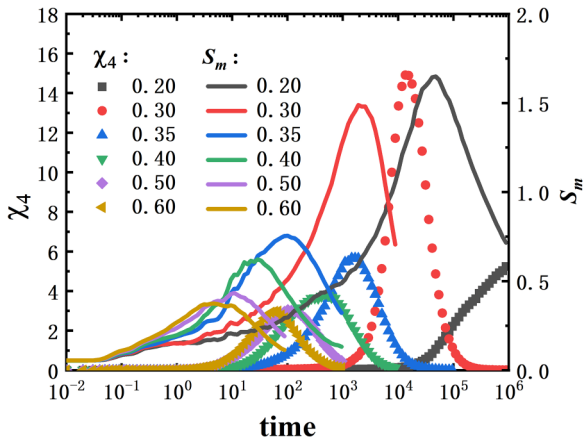

FIG. 2. The average skewness $S_m(t)$ (solid lines, right axis) and the dynamical susceptibility $\chi_4(t)$ (scatterd points, left axis) as a function of time. Different colors represent different temperatures.

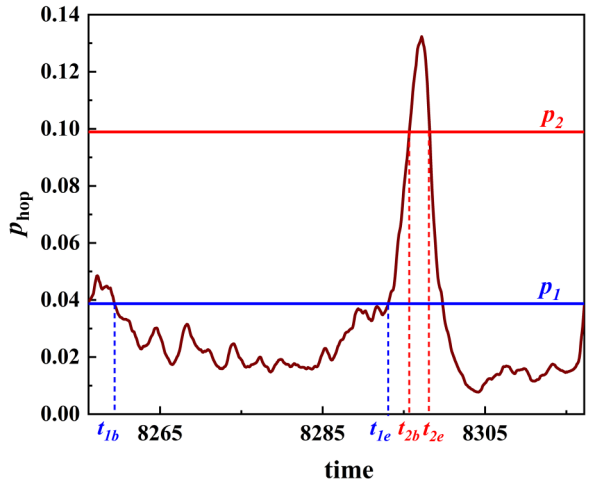

FIG. 3. The hopping function $p_{\text{hop},i}(t)$ of a particle during a cage-jumping event. p_2 (red horizontal line) is used to determine the occurence of a hopping (between $[t_{2b}, t_{2e}]$), and p_1 (blue horizontal line) is used to determine the quiescent period before the hopping (between $[t_{1b}, t_{1e}]$).

as

$$p_{\text{hop},i}(t) = \langle(\vec{r}_i - \langle\vec{r}_i\rangle_{N+1})^2\rangle_N^{\frac{1}{2}} \langle(\vec{r}_i - \langle\vec{r}_i\rangle_N)^2\rangle_{N+1}^{\frac{1}{2}}. \quad (2)$$

Here, $\vec{r}_i$ is the position of particle i, and N and $N+1$ are two adjacent time windows joined at time t. $\langle\ldots\rangle_N$ and $\langle\ldots\rangle_{N+1}$ represent time averages in the interval N and $N+1$, respectively. The durations of both time intervals are chosen as the inflection point of the mean squared displacement (MSD) or τ_h on double logarithmic plots [29]. Figure 3 shows a representative curve of the hopping function of a particle. During a cage-jumping event, a pronounced peak is observed in the p_{hop} plot. We use two threshold values p_1 and p_2 to better identify a cage-jumping event and the preceding quiescent period. Here p_1 is chosen as the MSD value at τ_h (blue horizontal line), and p_2 is chosen as the MSD value on the timescale of the peak of $\alpha_2(t)$ (red horizontal line) [30]. Cage jumping occurs when $p_{\text{hop},i}(t) \geqslant p_2$ ($t \in [t_{2b}, t_{2e}]$), where t_{2b} and t_{2e} indicate the beginning and the end of the hopping respectively (red dashed lines). Similarly, we define a quiescent period immediately before the hopping for $p_{\text{hop},i}(t) \leqslant p_1$ ($t \in [t_{1b}, t_{1e}]$) (blue dashed lines), when the particle fluctuates around an equilibrium position. Local structures around the particle are relatively stable during the quiescent period, and the local potential energy landscape can be mapped out by measuring the probability distribution around the equilibrium position. We define the positional fluctuation of particle i as $\Delta\vec{x}_i = \vec{x}_i - \langle\vec{x}_i\rangle_{t_q}$ where t_q is the duration of the quiescent period, and $\vec{x}_i$ is the position vector of particle i. The projection of $\Delta\vec{x}_i$ along a certain direction θ is then $\Delta x_{i,\theta}$. Under the harmonic approximation, the probability density of $\Delta x_{i,\theta}$ follows the Boltzmann distribution with $P_i(\Delta x_{i,\theta}) \propto \exp(-\frac{k_{i,\theta}\Delta x_{i,\theta}^2}{2k_BT})$, where $k_{i,\theta} = \frac{k_BT}{\langle\Delta x_{i,\theta}^2\rangle_{t_q}}$ is the stiffness coefficient of the potential energy along direction θ. $k_{i,\theta}$ measures the resistance a particle meets when moving toward direction θ. Figure 4(a) plots the angular distribution of $k_{i,\theta}$ of a randomly selected particle, where anisotropy is evident.

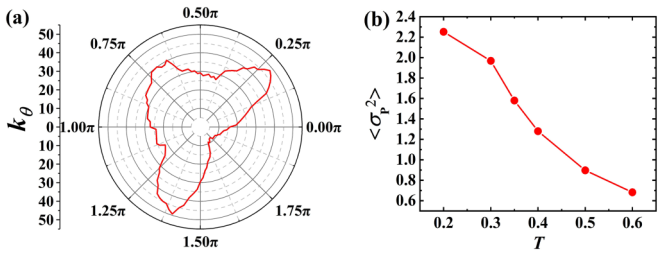

FIG. 4. Anisotropy in local potential energy landscapes. (a) The angular distribution of a particle's stiffness k_θ. The left vertical axis represents the radial coordinate. (b) Averaged angular anisotropy of the local potential energy landscape as a function of temperature in simulations.

The cage-jumping probability in a certain direction is directly related to the stiffness anisotropy in local structures, with particles more likely to overcome softer barriers. We can thus define an expected relative probability along direction θ at a given temperature as

$$P_{\theta,\text{expect}} = P_0 \exp(-k_\theta a^2/2k_BT) \quad (3)$$

where k_B is the Boltzmann constant, T is the temperature, a is the typical cage-jumping length scale chosen to be half of the particle radius, and $P_0 = \sum_\theta \exp(-k_\theta a^2/2k_BT)$ is a normalization factor. The anisotropy of $P_{\theta,\text{expect}}$ can be evaluated by its angular fluctuation:

$$\sigma_P^2 = \frac{\langle P_{\theta,\text{expect}}^2\rangle_\theta - \langle P_{\theta,\text{expect}}\rangle_\theta^2}{\langle P_{\theta,\text{expect}}\rangle_\theta^2}. \quad (4)$$

Figure 4(b) plots the angular anisotropy of local potential energy landscapes averaged over all particles $\langle\sigma_P^2\rangle$ at different temperatures in simulations. The averaged anisotropy in the local potential energy landscape decreases with temperature, in agreement with the temperature dependence of diffusion anisotropy observed in Fig. 2.

Particle-level correlations between stiffness anisotropy and diffusion anisotropy can be evaluated by comparing the distributions of displacement directions during cage-jumping events and the expected probability probability defined by Eq. (3). The expected cage-jumping probability distribution $P_{\theta,\text{expect}}$ is first compared to a baseline of uniform random distribution $P_{\theta,\text{random}} \equiv 1/120$, as the directions are partitioned into 120 sectors in our current work. The directions where $P_{\theta,\text{expect}} > P_{\theta,\text{random}}$ are defined as favored directions, or Θ, and the expected probability of cage jumping in favored directions is $P_{\text{expect}}(\Theta) = \sum_{\theta\in\Theta} P_{\theta,\text{expect}}$. The probability of actual jumping events in the directions of Θ, $P_{\text{actual}}(\Theta)$, can be obtained by averaging over a large number of observations. $P_{\text{actual}}(\Theta) > P_{\text{random}}(\Theta)$ indicates that particles tend to move in the directions favored by stiffness distributions. And in the case where the cage jumping always occurs in the favored directions, we have $P_{\text{actual}}(\Theta) = P_{\text{expect}}(\Theta)$. Therefore, we can define a correlation coefficient that measures the predicting power of $P_{\theta,\text{expect}}$, with

$$R = \frac{P_{\text{actual}}(\Theta) - P_{\text{random}}(\Theta)}{P_{\text{expect}}(\Theta) - P_{\text{random}}(\Theta)}. \quad (5)$$

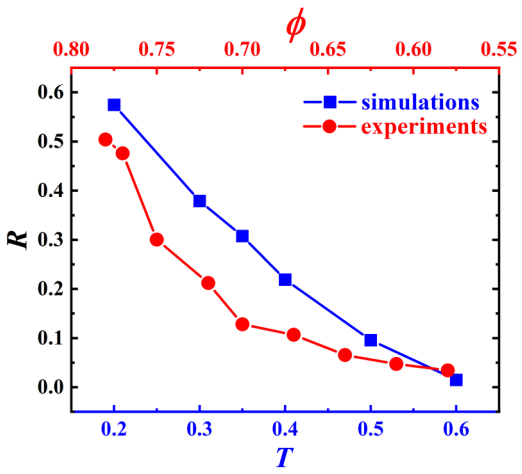

FIG. 5. Correlation coefficient between cage-jumping directions and the expected directions from local stiffness distributions in the simulations (blue squares) and experiments (red circles) as a function of temperature T or packing fraction ϕ.

$R = 0$ when the directions of cage jumping are completely random, and $R = 1$ when the directions of cage jumping are determined by the expected probability from the local potential energy landscape, or structures. Figure 5 plots the correlation coefficient in the simulations (blue squares) and experiments (red circles) as a function of temperature or packing fraction. As expected, the predicting power of the local potential energy landscape increases with decreasing temperature or increasing packing fraction. In particular, at the lowest temperature, the correlation coefficient is close to 60%, which is significant considering the stochastic nature of particle motion in liquids and glasses.

In our simulations, the anisotropy of diffusion is not spatially correlated to the rate of diffusion, despite both being connected to the softness in the potential energy landscape. We employ the dynamic propensity to measure the diffusion rate of individual particles. The dynamic propensity is defined as $h_i(t) = \langle[\vec{r}_i(t) - \vec{r}_i(0)]^2\rangle_{\text{isoc}}$, which is the ensemble-averaged mean squared displacement of a particle [8,14]. Figure 6 shows the spatial distribution of $s_{m,i}(\tau_m)$ and $h_i(\tau_m)$ for temperature $T_e = 0.3$. Here τ_m is chosen to be the time when $S_m(t)$ reaches the peak. The spatial distribution of the propensity is highly correlated, with large clusters of high propensity regions, in agreement with previous reports [25,31–36]. On the other hand, the spatial distribution of the skewness is much more scattered, with high skewness regions uniformly distributed in the system. The different spatial distributions of the diffusion anisotropy and the dynamic propensity reflect the different aspects of the local energy landscape from which they originate. The dynamic propensity depends on the heterogeneity of the potential energy landscape on large length scales, while the diffusion anisotropy depends on the shape of the local energy landscape. These two characteristics of the local energy landscape are not necessarily correlated. For example, a liquidlike region may have similarly low energy barriers in all directions, while a particle may be trapped in a highly anisotropic region where even the softest barriers are still too high to overcome in a short period of time.

In addition to decoupled spatial distributions between diffusion anisotropy and diffusion rate, the characteristic timescales of these dynamic properties are also completely separated. The symbols in Fig. 2 show the ensemble-averaged dynamical susceptibility χ_4 and diffusion anisotropy S_m as a function of time at different temperatures. χ_4 is defined as

$$\chi_4(t) = \frac{1}{N}\left[\left\langle Q_m^2(t)\right\rangle_{\text{isoc}} - \left\langle Q_m(t)\right\rangle_{\text{isoc}}^2\right] \tag{6}$$

where $Q_m(t) = \sum_i^N \exp(-\frac{\Delta x_i(t)}{d^2})$, $\Delta x_i(t)$ is the displacement of particle i in a time window of t, and d is a preselected length scale which is chosen to be the first peak of the pair correlation function $g(r)$. This definition of χ_4 is similar to the one commonly used in glassy systems, except that both $Q_m^2(t)$ and $Q_m(t)$ are ensemble averaged over 5000 individual runs from the same initial configuration. For all the temperatures, the diffusion anisotropy peaks at timescales one or two orders of magnitude shorter than that for the dynamical susceptibility. Remarkably, when diffusion orientations are most anisotropic, the diffusion rate is spatially homogeneous, and when the diffusion rate is most heterogeneous, diffusions orientations are almost isotropic. Therefore, anisotropic diffusions do not necessarily lead to spatially heterogeneous

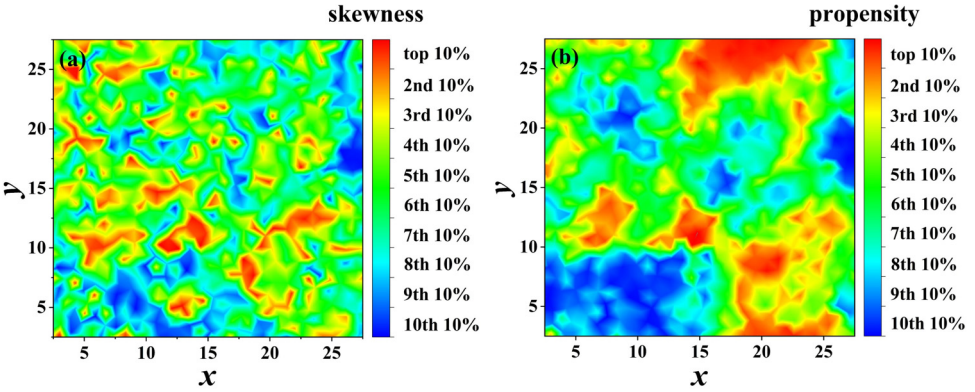

FIG. 6. The spatial distributions of the maximum skewness $s_{m,i}$ (a) and dynamic propensity h_i (b) in isoconfigurational simulations. The temperature is $T_e = 0.3$, and the timescale τ_m is the time when $S_m(t)$ reaches the peak.

dynamics, and diffusion anisotropy cannot be readily deduced from the observed dynamical heterogeneity.

IV. CONCLUSIONS

In conclusion, using isoconfigurational ensemble simulations and colloidal experiments, we show that as the system enters the supercooled regime, not only does the rate of diffusion become spatially heterogeneous, but the diffusion directions for individual particles are also anisotropic. The dynamical heterogeneity and diffusion anisotropy originate from the complex energy landscape at different length scales, which begins to develop in supercooled liquids. The rate of diffusion is faster in regions of lower energy barriers, while local hoppings prefer directions with relatively soft constraints. As the shape of the energy landscape can, in principle, be inferred from local structures, the evolution of the structure in supercooled liquids can be predicted probabilistically by estimating the hopping probability and the likely hopping directions for each particle. In particular, particles with low energy barriers for rearrangement and high hopping anisotropy contribute the most to the changes of system configurations, and may hold the key to understanding the evolution of structures and dynamics in supercooled liquids.

ACKNOWLEDGMENTS

This work was supported by the National Natural Science Foundation of China (Grant No. 12174434).

DATA AVAILABILITY

The data that support the findings of this article are not publicly available. The data are available from the authors upon reasonable request.

[1] A. Heuer and K. Okun, Heterogeneous and homogeneous dynamics in a simulated polymer melt: Analysis of multi-time correlation functions, J. Chem. Phys. **106**, 6176 (1997).

[2] W. Kob, C. Donati, S. J. Plimpton, P. H. Poole, and S. C. Glotzer, Dynamical heterogeneities in a supercooled Lennard-Jones liquid, Phys. Rev. Lett. **79**, 2827 (1997).

[3] E. R. Weeks, J. C. Crocker, A. C. Levitt, A. Schofield, and D. A. Weitz, Three-dimensional direct imaging of structural relaxation near the colloidal glass transition, Science **287**, 627 (2000).

[4] M. D. Ediger, Spatially heterogeneous dynamics in supercooled liquids, Annu. Rev. Phys. Chem. **51**, 99 (2000).

[5] N. Lačević, F. W. Starr, T. Schrøder, and S. C. Glotzer, Spatially heterogeneous dynamics investigated via a time-dependent four-point density correlation function, J. Chem. Phys. **119**, 7372 (2003).

[6] O. Dauchot, G. Marty, and G. Biroli, Dynamical heterogeneity close to the jamming transition in a sheared granular material, Phys. Rev. Lett. **95**, 265701 (2005).

[7] Y. Rahmani, K. Van Der Vaart, B. Van Dam, Z. Hu, V. Chikkadi, and P. Schall, Dynamic heterogeneity in hard and soft sphere colloidal glasses, Soft Matter **8**, 4264 (2012).

[8] A. Widmer-Cooper, P. Harrowell, and H. Fynewever, How reproducible are dynamic heterogeneities in a supercooled liquid?, Phys. Rev. Lett. **93**, 135701 (2004).

[9] H. Tanaka, T. Kawasaki, H. Shintani, and K. Watanabe, Critical-like behaviour of glass-forming liquids, Nat. Mater. **9**, 324 (2010).

[10] H. Tong and N. Xu, Order parameter for structural heterogeneity in disordered solids, Phys. Rev. E **90**, 010401(R) (2014).

[11] X. Yang, R. Liu, M. Yang, W.-H. Wang, and K. Chen, Structures of local rearrangements in soft colloidal glasses, Phys. Rev. Lett. **116**, 238003 (2016).

[12] T. Kawasaki, T. Araki, and H. Tanaka, Correlation between dynamic heterogeneity and medium-range order in two-dimensional glass-forming liquids, Phys. Rev. Lett. **99**, 215701 (2007).

[13] K. Watanabe and H. Tanaka, Direct observation of medium-range crystalline order in granular liquids near the glass transition, Phys. Rev. Lett. **100**, 158002 (2008).

[14] H. Tong and H. Tanaka, Revealing hidden structural order controlling both fast and slow glassy dynamics in supercooled liquids, Phys. Rev. X **8**, 011041 (2018).

[15] K. Chen, W. G. Ellenbroek, Z. Zhang, D. T. Chen, P. J. Yunker, S. Henkes, C. Brito, O. Dauchot, W. van Saarloos, A. J. Liu, and A. G. Yodh, Low-frequency vibrations of soft colloidal glasses, Phys. Rev. Lett. **105**, 025501 (2010).

[16] K. Chen, M. L. Manning, P. J. Yunker, W. G. Ellenbroek, Z. Zhang, A. J. Liu, and A. G. Yodh, Measurement of correlations between low-frequency vibrational modes and particle rearrangements in quasi-two-dimensional colloidal glasses, Phys. Rev. Lett. **107**, 108301 (2011).

[17] S. Slotterback, M. Toiya, L. Goff, J. F. Douglas, and W. Losert, Correlation between particle motion and Voronoi-cell-shape fluctuations during the compaction of granular matter, Phys. Rev. Lett. **101**, 258001 (2008).

[18] Y. Xia, X. Yang, J. Huang, R. Liu, N. Xu, M. Yang, and K. Chen, Orientational order in dense colloidal liquids and glasses, Phys. Rev. Lett. **131**, 128201 (2023).

[19] R. Brüning, D. A. St-Onge, S. Patterson, and W. Kob, Glass transitions in one-, two-, three-, and four-dimensional binary Lennard-Jones systems, J. Phys.: Condens. Matter **21**, 035117 (2008).

[20] E. Flenner and G. Szamel, Fundamental differences between glassy dynamics in two and three dimensions, Nat. Commun. **6**, 7392 (2015).

[21] E. Bitzek, P. Koskinen, F. Gähler, M. Moseler, and P. Gumbsch, Structural relaxation made simple, Phys. Rev. Lett. **97**, 170201 (2006).

[22] P. J. Yunker, K. Chen, M. D. Gratale, M. A. Lohr, T. Still, and A. Yodh, Physics in ordered and disordered colloidal matter composed of poly (*N*-isopropylacrylamide) microgel particles, Rep. Prog. Phys. **77**, 056601 (2014).

[23] J. C. Crocker and D. G. Grier, Methods of digital video microscopy for colloidal studies, J. Colloid Interface Sci. **179**, 298 (1996).

[24] W. K. Kegel and A. van Blaaderen, Direct observation of dynamical heterogeneities in colloidal hard-sphere suspensions, Science **287**, 290 (2000).

[25] C. Donati, S. C. Glotzer, P. H. Poole, W. Kob, and S. J. Plimpton, Spatial correlations of mobility and immobility in a glass-forming Lennard-Jones liquid, Phys. Rev. E **60**, 3107 (1999).

[26] Z. Zheng, F. Wang, and Y. Han, Glass transitions in quasi-two-dimensional suspensions of colloidal ellipsoids, Phys. Rev. Lett. **107**, 065702 (2011).

[27] R. Candelier, A. Widmer-Cooper, J. K. Kummerfeld, O. Dauchot, G. Biroli, P. Harrowell, and D. R. Reichman, Spatiotemporal hierarchy of relaxation events, dynamical heterogeneities, and structural reorganization in a supercooled liquid, Phys. Rev. Lett. **105**, 135702 (2010).

[28] A. Smessaert and J. Rottler, Distribution of local relaxation events in an aging three-dimensional glass: Spatiotemporal correlation and dynamical heterogeneity, Phys. Rev. E **88**, 022314 (2013).

[29] X. Ma, Z. S. Davidson, T. Still, R. J. Ivancic, S. S. Schoenholz, A. J. Liu, and A. G. Yodh, Heterogeneous activation, local structure, and softness in supercooled colloidal liquids, Phys. Rev. Lett. **122**, 028001 (2019).

[30] M. Sharma, M. K. Nandi, and S. M. Bhattacharyya, Identifying structural signature of dynamical heterogeneity via the local softness parameter, Phys. Rev. E **105**, 044604 (2022).

[31] C. Donati, J. F. Douglas, W. Kob, S. J. Plimpton, P. H. Poole, and S. C. Glotzer, Stringlike cooperative motion in a supercooled liquid, Phys. Rev. Lett. **80**, 2338 (1998).

[32] Y. Gebremichael, M. Vogel, and S. C. Glotzer, Particle dynamics and the development of string-like motion in a simulated monoatomic supercooled liquid, J. Chem. Phys. **120**, 4415 (2004).

[33] W. Kob, S. Roldán-Vargas, and L. Berthier, Non-monotonic temperature evolution of dynamic correlations in glass-forming liquids, Nat. Phys. **8**, 164 (2012).

[34] S. Gokhale, K. Hima Nagamanasa, R. Ganapathy, and A. Sood, Growing dynamical facilitation on approaching the random pinning colloidal glass transition, Nat. Commun. **5**, 4685 (2014).

[35] F. W. Starr, J. F. Douglas, and S. Sastry, The relationship of dynamical heterogeneity to the Adam-Gibbs and random first-order transition theories of glass formation, J. Chem. Phys. **138**, 12A541 (2013).

[36] K. H. Nagamanasa, S. Gokhale, A. Sood, and R. Ganapathy, Direct measurements of growing amorphous order and non-monotonic dynamic correlations in a colloidal glass-former, Nat. Phys. **11**, 403 (2015).